

A near-infrared and *UBVRI* photometric analysis of the open cluster IC 361

G C Joshi*

Department of Physics, Govt. Degree College, Kotdwar-Bhabar, Pauri, Uttarakhand 246149, India

Received: 12 June 2020 / Accepted: 25 January 2021 / Published online: 9 March 2021

Abstract: A detailed optical and infrared photometric analysis of the open star cluster IC 361 is given in the present paper. On studying the radial density profile, radial extent of the cluster is found to be 8.0 ± 0.5 arcmin. The basic physical parameters of the cluster such as $E(B - V) = 0.56 \pm 0.10$ mag, $E(V - K) = 1.72 \pm 0.12$ mag, $\log(\text{Age}) = 9.10 \pm 0.05$, and $(m - M)_0 = 12.54 \pm 0.05$ mag are obtained using the colour–colour and colour–magnitude diagrams. IC 361 is found to be located at a distance of 3.22 ± 0.07 kpc. Using the archival proper motion catalogues, we estimate the mean proper motions of IC 361 as 4.97 ± 0.17 mas yr⁻¹ and -5.80 ± 0.18 mas yr⁻¹ in the direction of RA and Dec, respectively. A uniform distribution of mass between small scale and large scale is confirmed by MF slope of IC 361. However, the mass function slope of cluster region is found to be -1.06 ± 0.09 , which is too low compared to the Salpeter value. Our study is further showing a dynamical relaxation behaviour of the cluster IC 361.

Keywords: Milky way: Open star cluster; Individual: IC 361; Method-data analysis (98.35.-a; 98.62.Ai; 98.65.-r); Astrometry (95.10.JK); Astronomical observations (95.85.-e)

1. Introduction

The physical quantities of an individual star cluster are required to understand the processes of star formation and stellar evolution in the galaxy. For this purpose, author selected an open cluster (OC) IC 361 of Camelopardalis constellation [1]. Since observed regions of clusters are contaminated by the field stars, therefore, a comprehensive membership analysis is needed to confirm the stellar membership of clusters and to decide their periphery. In the case of IC 361, it is well detached from the field stars and poorly studied due to its faintness [2]. It lies in the second galactic quadrant. A considerable interstellar reddening is demonstrated by IC 361 due to the presence of immediate vicinity of the Camelopardalis dark clouds [3]. It is approximately 2.5 kpc away from Earth, and it shows the high value of reddening, $E_{B-V} = 0.55$, with the age range from 0.5 to 1 Gyr [1]. A deep and multi-colour photometry of IC 361 is needed to precise determination of fundamental parameters and its dynamical behaviour. On this

background, the comprehensive analysis of *UBVRI* and *JHK* photometric data is carried out in the present study.

This paper is organized as follows: The photometric observation of the cluster is described in Sect. 2. The centre coordinates and size of cluster IC 361 are computed in Sect. 3. The results of parameters through colour–magnitude diagrams (CMDs) and two colour diagrams (TCDs) analysis are given in Sect. 4. Section 5 is devoted to identify the probable members of IC 361 and its mean proper motions. Dynamical study of the cluster has been carried out in Sect. 6. The final conclusions and discussion are stated in Sect. 7.

2. Photometric observation and comparison with previous study

Johnson-Cousins *UBVRI* photometry of stars in the field of IC 361 was obtained on 24 December 2013, using the 1.04-m Sampurnanand telescope at Nainital, India. The observation details of this cluster are given in Table 1. On the same night, we also observed Landolt's standard field: SA92 [4]. A total of 24 standard stars are identified in the field of view (FOV) of SA92 and their air-mass ranges from 1.01 to 3.41. The usual image processing procedures

*Corresponding author, E-mail: gchandra.2012@rediffmail.com

Table 1 The observation details of IC 361

Photometric band	No. of frames	Time of observation (JD = 2456651+)	Exposure time (s)	Air-mass point	Zero coefficient	Colour coefficient	Extinction coefficient
U	1	0.27968	300	1.227	7.88 ± 0.01	-0.08 ± 0.03	0.26 ± 0.01
B	2	0.26235, 0.26404	30, 150	1.189, 1.194	5.33 ± 0.01	-0.06 ± 0.02	0.11 ± 0.00
V	2	0.26810, 0.27126	120,30	1.200, 1.204	4.74 ± 0.00	-0.09 ± 0.01	0.07 ± 0.00
R	1	0.27322	40	1.208	4.44 ± 0.01	-0.05 ± 0.01	0.04 ± 0.00
I	2	0.27513, 0.27690	25, 100	1.211, 1.216	4.91 ± 0.01	-0.06 ± 0.01	0.03 ± 0.00

The value of observation time, exposure time and air-mass has been given in the same order

(bias subtraction, flat fielding, and cosmic ray removal) were performed through IRAF¹ software package. Photometry of the frames was performed using the DAOPHOT II profile fitting software [5]. The resultant transformation coefficients for the standard stars are also listed in Table 1, and photometric error with magnitude is depicted in Fig. 1a. The rms scatter values of the transformation of standard photometry are found to be 0.037, 0.022, 0.005, 0.007 and 0.013 for *U*, *B*, *V*, *R* and *I* bands, respectively. The observed field of view (FOV) of the cluster is $\sim 13 \times 13$ arcmin², and we found 1883 stars in the FOV of the cluster.

In order to transform CCD pixel coordinates to celestial coordinates, we used the online digitized ESO catalogue (included in the skycut software) as an absolute astrometric reference frame. A linear astrometric solution was derived for the *V* filter reference frame by matching positions of 170 well-isolated bright stars. The *cmap* and *cctran* routines are utilized for this purpose. We found 276 common stars between present photometry and Vilnius photometry [3], and *V*-magnitude difference between these datasets is shown in Fig. 1b. The mean difference of both datasets is -0.001 mag, and its error is found to be 0.002 mag.

3. Centre and radius of the cluster

The centre coordinates (α, δ) of cluster IC 361 are found to be ($4^h 18^m 56^s \pm 0.2^s, +58^\circ 15' 18'' \pm 3''$). Similarly, the equivalent pixel coordinates of centre of observed reference of IC 361 frame are given as $(x, y) = (465 \pm 4, 545 \pm 4)$. The radial density profile (RDP) of open cluster is used to determine the cluster radius. The RDP is

constructed by determining the stellar density in concentric rings of equal width around the cluster centre. We choose a thickness of about 1 arcmin (~ 80 pixels) for each ring in order to have statistically significant number of stars in each radial zone. The stellar density (ρ_r) at the distance r from the cluster centre is defined by the following empirical formula [6]:

$$\rho_r = \rho_f + \frac{\rho_0}{1 + (\frac{r}{r_c})^2} \quad (1)$$

where ρ_0 is the field subtracted peak stellar density (max. model density) and ρ_f is the background density. The r_c is core radius of the cluster defined as a distance from the centre at which the density ρ_r becomes half of the ρ_0 . The cluster radius is determined where RDP intercepts the background density. The prescribed background density is estimated as the average of first three approximate values of field densities and estimated background stellar densities of utilized datasets of each catalogue, and is depicted by green line in each panel of Fig. 2, whereas the model stellar densities are depicted by the red lines. The present analysis indicates that the different seller numbers of different catalogues provide the different values of radius and are listed in Table 2. Resultant values are computed by taking the straight mean of the table values. Thus, the radius and core radius of IC 361 are found to be 8.24 ± 0.32 arcmin ($\sim 645 \pm 25$ pixels) and 2.34 ± 0.47 arcmin, respectively.

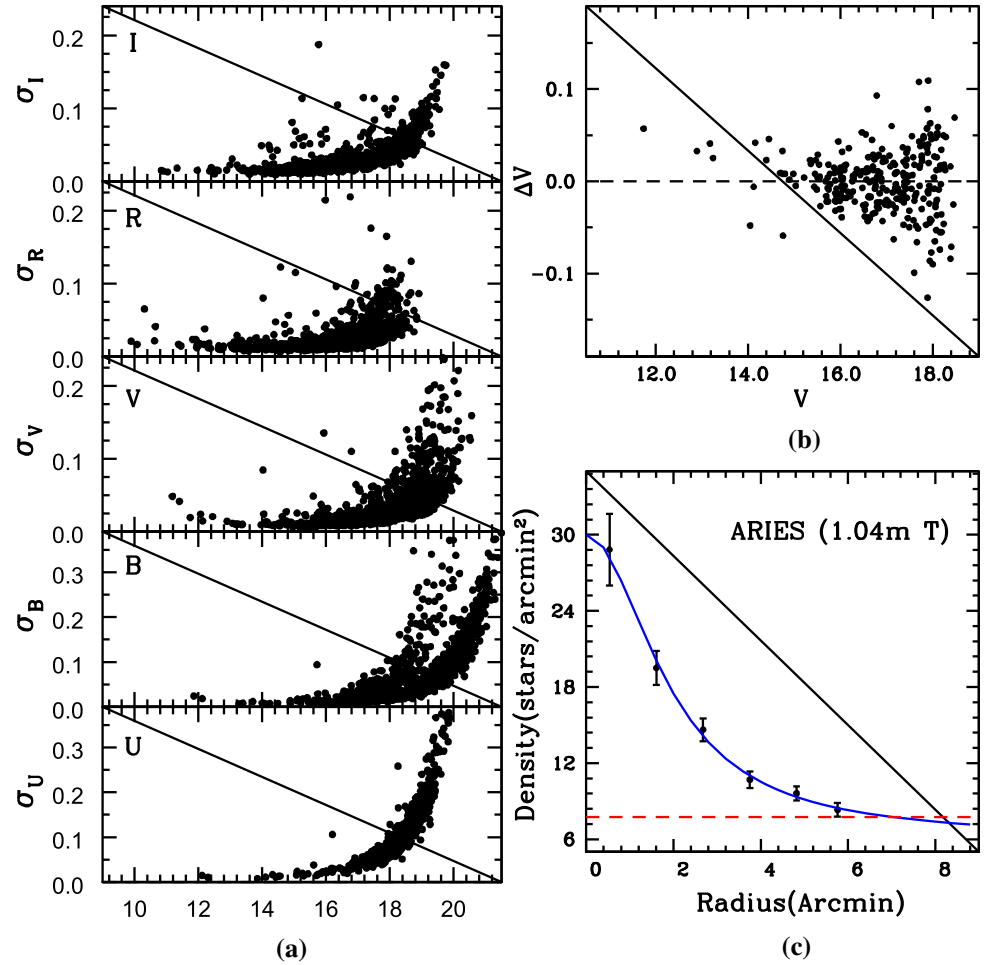
4. Analysis through the CMD and TCD

4.1. Nature of extinction law

As the light is emitted from the star cluster, the light or it passes through the interstellar dust and gas, scattering and absorption of light take place. Since the absorption and scattering of the blue light are more compared to the red

¹ Image Reduction and Analysis Facility (IRAF) is distributed by the National Optical Astronomy Observatories, which are operated by the Association of Universities for Research in Astronomy, Inc., under cooperative agreement with the National Science Foundation.

Fig. 1 (a) The photometric error of stars as a function of brightness in the *UBVRI* bands. (b) A comparison of our *V* observations with the *V*-magnitude of stars observed by Zdanavicius et al. 2010. The dashed line represents a zero-magnitude difference. (c) The stellar RDP of stars of the field of *IC 361*. The solid line represents the King profile, and the horizontal line shows the average field star density



light, the stars appear reddened. The law of selective absorption is the same for all directions of the galaxy. The ratio of total extinction (A_V) to reddening $[E(B - V)]$ is known to be total-to-selective-extinction ratio (R_V). The normal value of R_V comes to be 3.1 for galaxy, and it is known to be normal reddening law. Generally, normal reddening law is applicable when dust and intermediate stellar gases are absent in the line of sight of the cluster [7]. However, the reddening law is expected to be different in the presence of dust grains. We have investigated the nature of reddening law using $(V - \lambda)/(B - V)$ TCDs [8], where λ is any broad band filter, namely *R, I, J, H, K, W₁, and W₂*. Here, W_1 and W_2 are mid-IR passbands used for wide-field IR Survey Explorer (WISE [9]). The $(V - \lambda)/(B - V)$ TCDs have been widely used to separate the influence of the extinction produced by the diffuse interstellar material from that of the intra-cluster medium [8]. Therefore, we constructed the resultant $(V - \lambda)/(B - V)$ diagram in different wavelength bands, as shown in Fig. 3a. A best linear fit in the TCD of cluster gives the value of slope (m_{cluster}) for the corresponding TCD. The resultant values of the m_{cluster} for seven colours are listed in

Table 3 along with their normal values. Our slopes are quite comparable with those obtained for the diffuse interstellar material.

A total-to-selective extinction R_{cluster} is determined using the following relation [10]

$$R_{\text{cluster}} = \frac{m_{\text{cluster}}}{m_{\text{normal}}} \times R_{\text{normal}}. \quad (2)$$

Assuming the value of R_{normal} for the diffuse interstellar material as 3.1, we determined R_{cluster} in the first five colours listed in Table 3. These values indicate that the value R_{cluster} is found to be high for the shorter effective wavelength with reference of *V* optical band, whereas the values of R_{cluster} are low for bands, having the high effective wavelength compared to the *V* optical band. The mean value of R_{cluster} is estimated as $R = 2.94 \pm 0.11$ for the cluster *IC 361* through the last four computed values of R_{cluster} ; moreover, this mean value of R_{cluster} is low than of normal reddening law.

After using the estimated value of R_{cluster} , author computed the distance of cluster as 3.37 ± 0.15 kpc. This value

Fig. 2 The radial density profiles of the cluster, IC 361 through various catalogues, namely (a) 2MASS, (b) VILNIOUS, (c) WISE and (d) PPMXL. The solid curve of each panel represents the King profile, and the red and green horizontal lines represent the average field star density ($f_0 + 3\sigma$) and the average of first three points of field densities, respectively. The field density of RDP of each panel is computed as the average mean of approximate similar data points of stellar densities

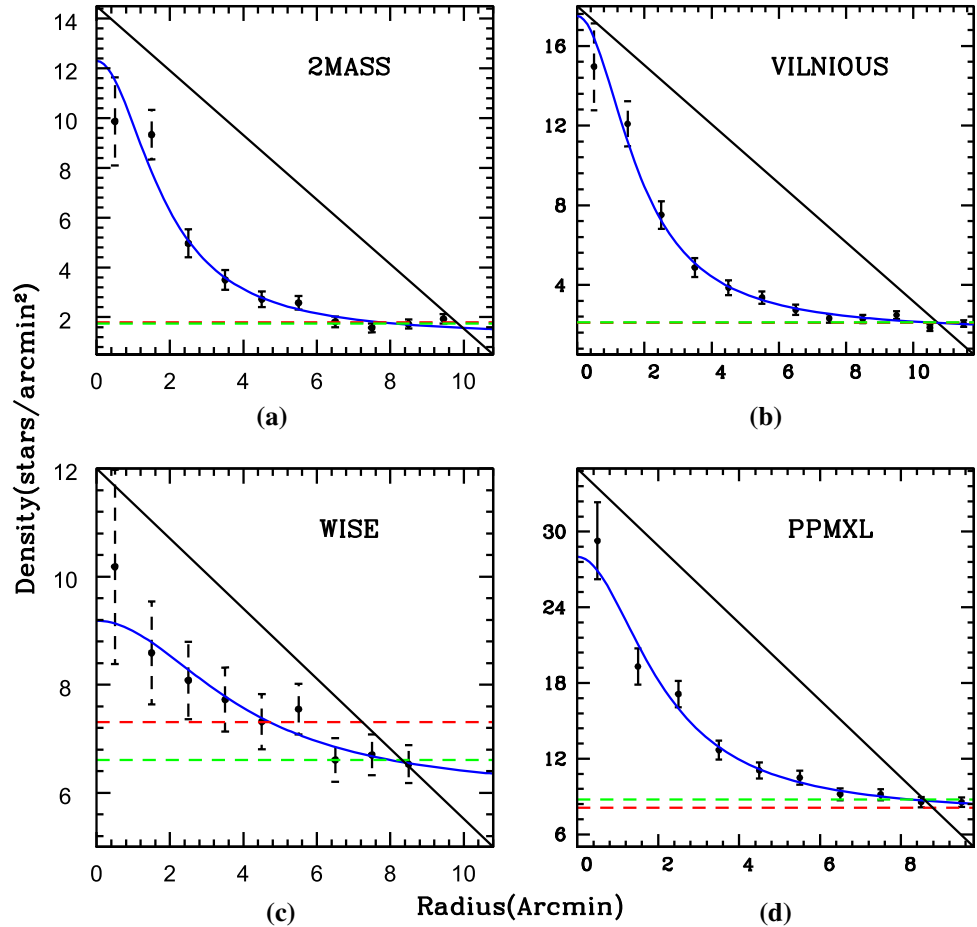


Table 2 The values of radius and core radius value of IC 361 as estimated by various extracted/estimated photometric datasets of catalogues/observatory

Radius (in arcmin)	Core radius (in arcmin)	Max. model density (St. No./arcmin ²)	Av. field density (St. No./arcmin ²)
<i>2MASS catalogue</i>			
8.0 ± 0.4	1.83 ± 0.34	11.08 ± 2.15	1.21 ± 0.19
<i>1.04-m telescope of ARIES</i>			
7.0 ± 0.2	1.91 ± 0.20	23.89 ± 1.76	6.11 ± 0.55
<i>PPMXL catalogue</i>			
8.2 ± 0.2	2.10 ± 0.24	20.48 ± 2.12	7.52 ± 0.29
<i>WISE catalogue</i>			
8.0 ± 0.4	3.99 ± 1.42	3.21 ± 0.51	5.97 ± 0.45
<i>Catalogue of VILNIOUS observatory</i>			
10.0 ± 0.4	1.85 ± 0.19	15.87 ± 1.74	1.63 ± 0.15

is 4.45% greater than the estimated distance by standard value of R_{normal} (given in Section 4.4).

4.2. $(U - B)$ vs $(B - V)$ TCD

The reddening, $E(B - V)$, in the cluster region, is estimated using the $(U - B)$ vs $(B - V)$ TCD. In Fig. 3b, we

plot TCD for the members found in our study. We also draw zero age-main sequence (ZAMS [11]) for observed MS stars on $(U - B)$ vs $(B - V)$ diagram. Here, we assume a solar metallicity for the cluster and a reddening vector of $E(U - B)/E(B - V) = 0.72$ [12]. The error of estimated reddening is calculated by using the relation [13]

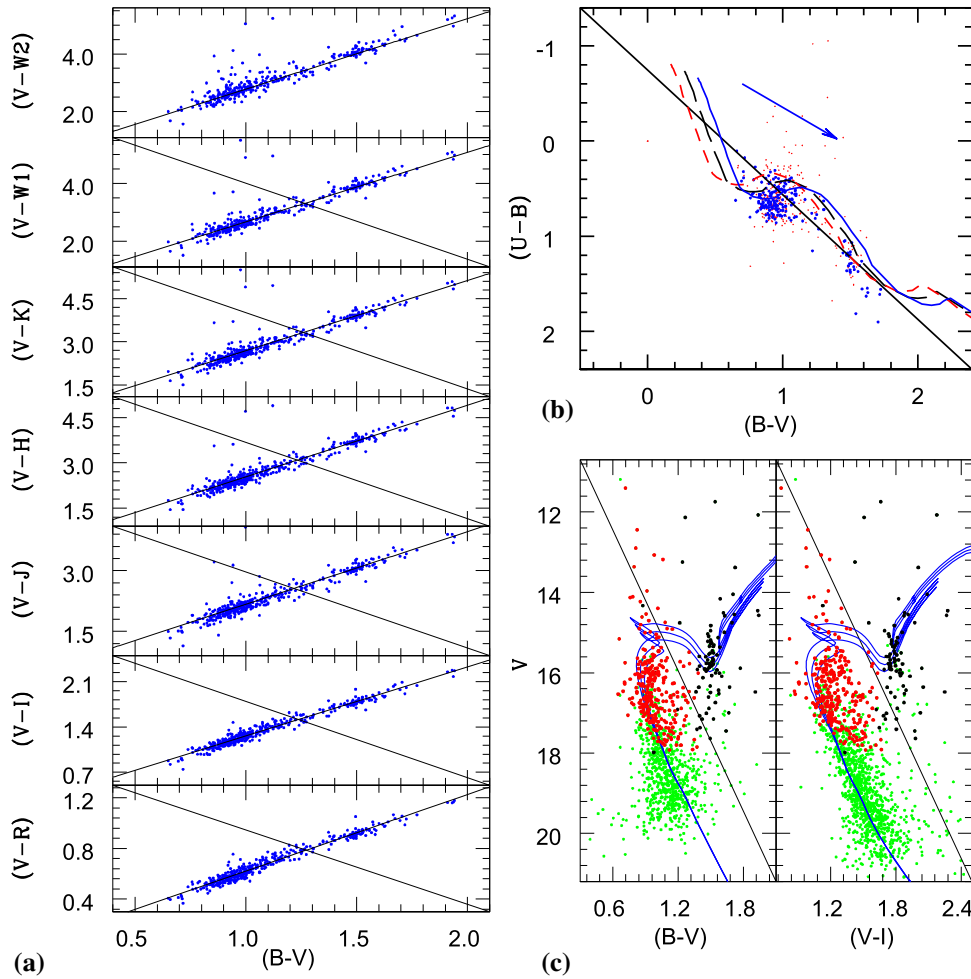


Fig. 3 (a) $(B - V)$ vs $(V - \lambda)$ diagrams, where λ represents $R, I, J, H, K, W_1,$ and W_2 . (b) $(B - V)$ vs $(U - B)$ colour-colour diagram for the cluster IC 361. For clarity, stars having an error in the U filter $eU > 0.05$ mag are not shown. The arrow shows the slope of normal reddening vector $E(U - B)/E(B - V) = 0.72$. The dashed black line shows the best fit taken in account of 0.56 and 0.40 mag shift in $(B - V)$ and $(U - B)$, respectively, while blue and red lines represent an error of ± 0.10 in the reddening vector. (c) $(B - V)/V$ and $(V - I)/V$ CMDs in the field of cluster IC 361. The solid line represents the best-

fit isochrone to the cluster for $\log(\text{Age}) = 9.1 \pm 0.05$ and $(m - M) = 14.4$ mag. The red and black dots represent the probable members and giant members of IC 361, having V -magnitude greater than 18 mag and found through the statistically cleaned approach as discussed in Sect. 5. The members of studied cluster have divided into probable members and giant members by the CMR value of CMRD approach as discussed in Sect. 5. Similarly, green dots represent the all identified stars in the direction of field of view of the open cluster IC 361

$$\sigma_{E(B-V)_{\text{sys}}}^2 = \sigma_{(U-B)_0}^2 + \sigma_{(B-V)_0}^2 + \sigma_{\text{vector}}^2. \quad (3)$$

The derived reddening $E(B - V)$ from our study is 0.56 ± 0.10 . The colour excesses $E(V - R)$ and $E(V - I)$ are estimated by the relations $E(V - R) = 0.60 \times E(B - V)$ [14] and $E(V - I) = 1.25 \times E(B - V)$ [15], respectively. In this connection, the values of colour excesses of $E(V - R)$ and $E(V - I)$ are computed to be 0.33 ± 0.06 and 0.7 ± 0.12 mag, respectively.

4.3. Reddening in near-infrared bands

The two-colour diagrams (TCDs) plots of various sets of two colours (magnitude difference of two bands) are

important tools for investigating the nature of extinction law, dependency with each other and their variation from normal values [16]. We are prescribing about two TCDs as below,

4.3.1. $(V - K)$ vs $(J - K)$ TCD

A $(V - K)$ vs $(J - K)$ diagram is used to determine the interstellar extinction in the near-IR (NIR) range. In Fig. 4a, we plot $(V - K)$ vs $(J - K)$ diagram, where we also overplot Marigo isochrones of solar metallicity by shifting the line in the direction of reddening vector $\frac{E(J-K)}{E(V-K)} = 0.173$. In this way, we obtained colour excesses of $E(V - K) = 1.72 \pm 0.05$ mag and $E(J - K) = 0.29 \pm$

Table 3 The slopes of the $(\lambda - V)/(B - V)$ TCDs in the direction of the cluster IC 361

Colour ratio	Normal value	Estimated value	Total-to-selective extinction value
$\frac{R-V}{B-V}$	0.55	0.60 ± 0.01	3.38
$\frac{I-V}{B-V}$	1.10	1.06 ± 0.01	2.99
$\frac{J-V}{B-V}$	1.96	1.79 ± 0.05	2.83
$\frac{H-V}{B-V}$	2.42	2.37 ± 0.05	3.03
$\frac{K-V}{B-V}$	2.60	2.44 ± 0.05	2.91
$\frac{W_1-V}{B-V}$	–	2.45 ± 0.07	–
$\frac{W_2-V}{B-V}$	–	2.41 ± 0.07	–

Their normal values are also given in the second column

0.03 mag. The relation $R = 1.1 \times \frac{E(V-K)}{E(B-V)}$ [17] was used to estimate the corresponding value of reddening. In Fig. 4a, we draw reddening vectors $\frac{E(V-K)}{E(B-V)}$ by shifting for the reddening values in the NIR bands (continuous line) and optical bands (long-dashed line). We yield $E(B - V) = 0.62 \pm 0.03$ mag in the direction of the cluster, which is slightly higher than that was determined in the optical band. One possibility for the discrepancy is the presence of a small IR excess for stars in the cluster IC 361. However, excess emission in the cluster IC 361 is not consistent with many relatively young clusters. Thus, IC 361 is an old age cluster with low IR-excess.

4.3.2. $(B - V)$ vs $(J - K)$ TCD

$(B - V)$ vs $(J - K)$ TCD of IC 361 is shown in Fig. 4b. The Marigo isochrone is used to know the relationship between $E(B - V)$ and $E(J - K)$. The colour excesses $E(B - V)$ and $E(J - K)$ of IC 361 are found to be 0.56 and 0.30 mag, respectively. As a result, the $E(J - K)/E(B - V)$ ratio for IC 361 is computed to be 0.54, which is close to the literature value, i.e. 0.56 [16]. This variation is possible due to the different value of total-to-selective-extinction from normal value. The red line of Fig. 4b represents Marigos isochrone without any shift, whereas the blue line shows the best-fitted line after shift of 0.56 mag in x -direction and 0.30 mag in y -direction, respectively.

4.4. Age and distance from CMDs

For the determination of age and distance of the cluster, we draw the $(B - V)/V$ and $(V - I)/V$ CMDs for probable members of cluster as illustrated in Fig. 3c. To find the probable members of IC 361, we use a radial cut to get rid of distant field stars. The value of radial cut is equivalent to the radius of cluster radius from the centre, and green dots of Fig. 3c represent those stars which are laying inside the cluster periphery of radial cut. For more precise calculation, author also used a statistical cleaning approach to get confirm probable members of cluster, and these confirm probable members of IC 361 which are depicted by the red dots in Fig. 3c. In this connection, the constructed CMDs

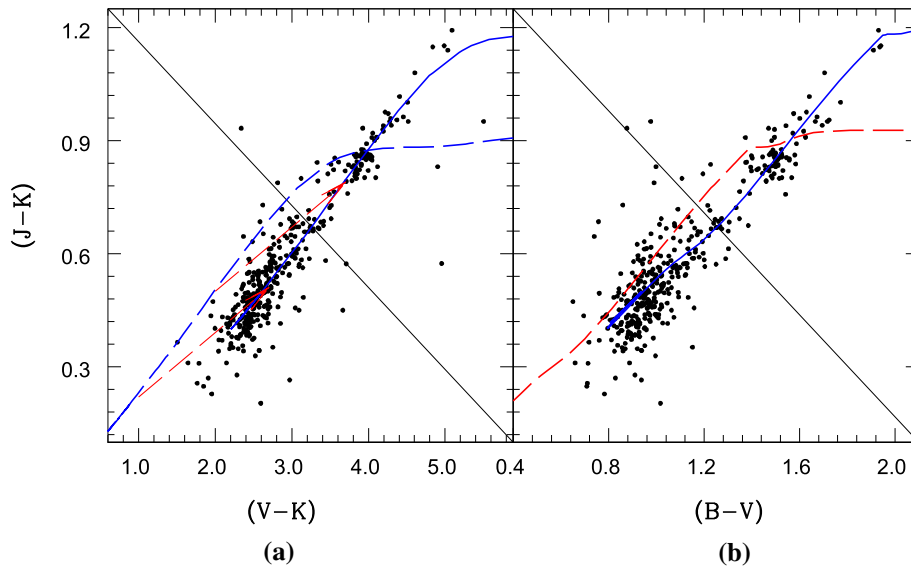


Fig. 4 (a) A $(V-K)$ vs $(J-K)$ diagram to determine interstellar extinction is shown in the left panel. The blue dashed line represents Marigo's isochrones of solar metallicity without any shift in colour, while blue solid line represents best-fitted line after shift of 1.72 mag in x -direction and 0.30 mag in y -direction. Two red arrows represent the reddening vector $\frac{(J-K)}{V-K} = 0.173$. (b) A $(B-V)$ vs $(J-K)$ diagram is

depicted in the right panel. The red dashed line represents Marigo's isochrones of solar metallicity without any shift in colour, while blue solid line represents best-fitted line after shift of 0.56 mag in x -direction and 0.30 mag in y -direction

show a well populated but broad main sequence (MS) star that may be due to photometric errors and/or presence of binary stars within the cluster. The variable reddening across the cluster region could also be the cause of the broad MS. We overplot Marigo's theoretical isochrones [18] on the CMDs by varying the distance modulus and age simultaneously in both $(B - V)/V$ and $(V - I)/V$ CMDs while keeping reddening $E(B - V) = 0.60$ mag and $E(V - I) = 0.75$ mag fixed as determined in the previous subsection and assuming $E(V - I) = 1.25 \times E(B - V)$. From the best visual isochrone fit to the varying age and distance combinations on the MS stars, we obtained a distance modulus $(V - M_V) = 14.4 \pm 0.10$ mag and $\log(\text{Age}) = 9.10 \pm 0.05$ (yr) for the cluster IC 361. Employing the correction for the reddening and assuming a normal reddening law (see Sect. 4.3), this corresponds to a true distance modulus $(m - M)_0 = 12.54 \pm 0.05$ mag or a distance of 3.22 ± 0.07 kpc for the cluster. Our estimated distance is close to the literature one, i.e. 3.3 kpc [2].

Though isochrone fitting is often used to estimate the age of the cluster in the absence of valuable spectroscopic

observations, it should be kept in mind that determining precise age through isochrone fitting in clusters, where no evolved stars are found, is very difficult as it contains a large uncertainty on this value.

5. Mean proper motion and probable members

The mean proper motion value of the cluster is the mean value of proper motion values of its probable members. Probable members of IC 361 are found through the field star decontamination. For this purpose, we have applied the CMRD [16] approach to find clear stellar sequence of studied cluster. The x -axis and y -axis of CMRD are the colour/magnitude ratio (CMR) and stellar V -magnitude, respectively. In the present case of IC 361, the values of stellar CMR have normalized stellar colour $(B - V)$ values with the V -magnitude. The CMR value is found to be 0.08 for brighter stars of cluster, and this value is used to separate cluster's stellar sequence from the field sequence as depicted in Fig. 5a. The cluster radius is found to be 8

Fig. 5 (a) The CMRD of IC 361 is shown in the upper left-hand panel. The red dots are depicted to the stellar branch of giant Stars. (b) The proper motion distribution of stars for IC 361. The red dots represent the statistically cleaned probable members used to determine the mean-proper motion, while the blue dots represent the probable members used to determine the mean proper motion of the cluster. (c) $(J-H)/J$ and $(J-K)/J$ CMDs in the field of cluster IC 361. The blue solid line represents the best-fit isochrone to the cluster for $\log(\text{Age}) = 9.1 \pm 0.05$ and $(m - M)_J = 12.87 \pm 0.04$ mag. (d) $(B-V)/V$ and $(V-I)/V$ CMDs in the field of cluster IC 361. The solid line represents the best-fit isochrone through $\log(\text{Age}) = 9.1 \pm 0.05$ and $(m - M)_V = 14.4$ mag

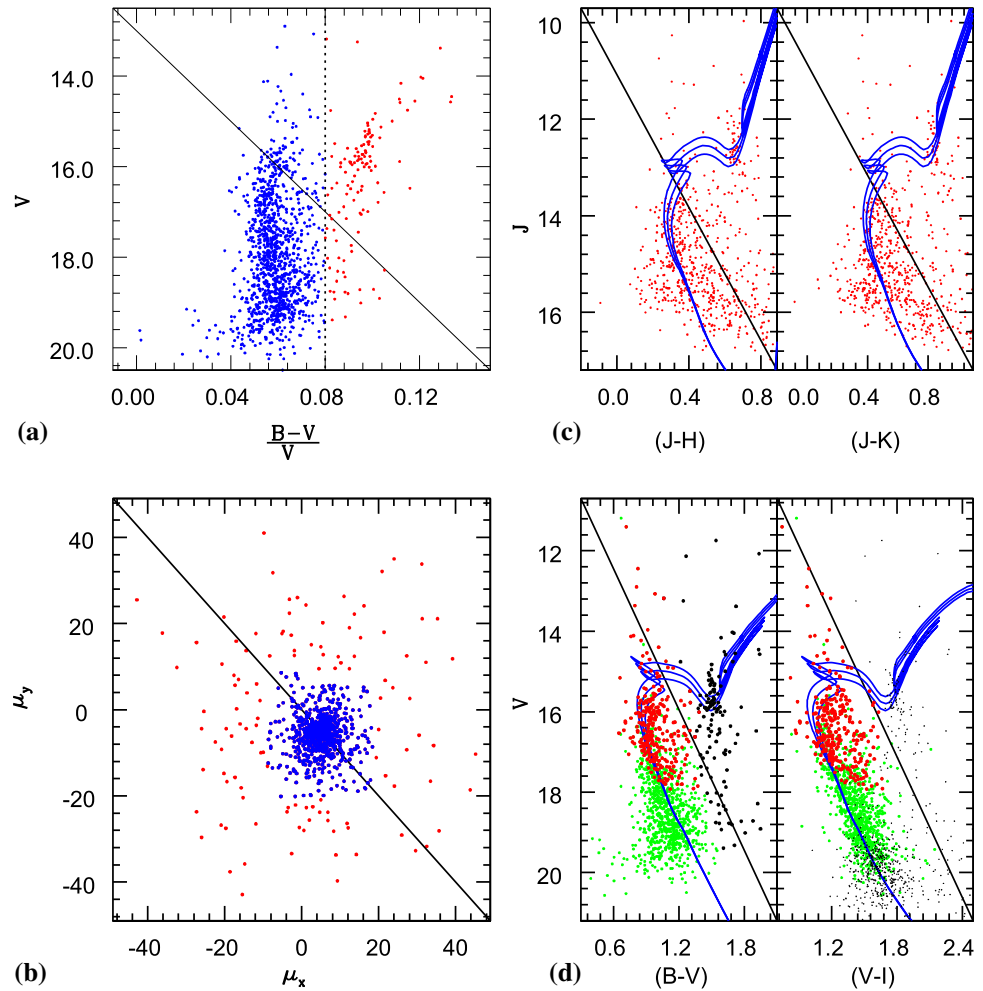


Table 4 The relative number of stars per unit volume of any cluster is defined as the mass function (MF), i.e. Φ

V range (mag)	Mass range M_{\odot}	\bar{m} M_{\odot}	$\log(\bar{m})$	N	$\log(\Phi)$	$e_{\log(\Phi)}$
13–14	2.160–2.345	2.252	0.353	045	3.103	0.149
14–15	2.149–2.160	2.155	0.333	110	4.696	0.095
15–16	1.878–2.149	2.014	0.304	203	3.540	0.070
16–17	1.573–1.878	1.726	0.237	305	3.598	0.057
17–18	1.312–1.573	1.443	0.159	386	3.690	0.051
18–19	1.104–1.312	1.208	0.082	283	3.578	0.059

In this table, the logarithm values of MF [$\log(\Phi)$] of the cluster IC 361 has been listed for different mass ranges of stars

arcmin in the present analysis or a diameter of 16 ± 1 arcmin. Since the estimated diameter is greater than the size of observed optical frame as well as other available optical catalogues, therefore, we cannot utilize these catalogues for statistical colour–magnitude cleaning [19] due to observations of limited region of cluster. The available *2MASS* data of field region of IC 361, however, does have a sufficiently wide field of view to satisfy our need. As a result, NIR *JHK* data of cluster is used to further decontamination of field stars. Since the required area of selected field region is equivalent to the enclosed area of cluster periphery, therefore, the disc size of field region for IC 361 is taken to be $10.0 \text{ arcmin} \leq r \leq 12.8 \text{ arcmin}$.

After iterating the cleaning procedure for each field region star, we found 850 probable members on the statistically cleaned CMDs [19]. The proper motion values of these probable members are extracted from the PPMXL catalogue [20], and the proper motion distribution of probable members is depicted in Fig. 5b. The x -axis and y -axis components of stellar proper motion are indicated by μ_x and μ_y , respectively, and these values are expressed as $\mu_x = \mu_{\alpha} \cos \delta$ and $\mu_y = \mu_{\delta}$. In the equatorial coordinate system, the prescribed μ_{α} and μ_{δ} are the components of proper motion in the direction of RA and Dec, respectively. Thus, μ_x is a shrink value of μ_{α} by a factor of $\cos \delta$ due to the changing angular size of circles of constant RA when moving from the celestial equator towards the celestial pole. Such shrinking effect of μ_{α} is known as the $\cos(\text{Dec})$ effect in the proper motion.

The location of these probable members around best-fitted isochrones of $(B - V)/V$ and $(J - K)/J$ CMDs confirms the main sequence of IC 361 in Fig. 5c, d. The resultant probable members are further utilized to estimate the mean proper motion of IC 361 through 3σ clipping approach. In this approach, the stars which do not fall within 3σ value of the mean are rejected for estimation. After 3σ clipping, we found 725 probable members to estimate the mean proper motion as depicted by blue dots in Fig. 5b. In this connection, the mean proper motion values of IC 361 are found to be $\bar{\mu}_x = 4.97 \pm 0.17 \text{ mas yr}^{-1}$

and $\bar{\mu}_y = -5.80 \pm 0.18 \text{ mas yr}^{-1}$ in RA and DEC directions, respectively.

6. Dynamical study of the cluster

6.1. Luminosity and mass functions

The luminosity function (LF) is the total number of cluster members in different magnitude bins. The estimated number of stars in each magnitude bin for the cluster (N_C) is given in Table 4. One can see that number of stars reduced significantly after the 19 mag, which is due to incompleteness factor. Artificial star tests [21] are used to determine incompleteness and to modify the photometric errors of science images. Such studies indicate that generally, the data incompleteness increases with the stellar faintness [22]. In the present catalogue, it is better than 90% up to 19 mag. In Fig. 5c, the green dots represent the identified stars in the FOV of IC 361 and the red dots represent the probable members of cluster. It is noted that the probable members are not appeared after 18 V-mag. The turn point of best-fitted isochrone on main sequence of IC 361 is found at near of 15 V-mag. Therefore, we have not applied any correction to the luminosity and mass functions between V-mag range 15–18 derived in the present study.

The initial mass function (IMF) is defined as the distribution of stellar masses per unit volume in a star formation event, and knowledge of IMF is very effective to determine the subsequent evolution of cluster. The direct measurement of IMF is not possible due to the dynamical evolution of stellar systems though we can estimate the present mass function (MF) of cluster. The MF is defined as the relative numbers of stars per unit mass and can be expressed by a power law $N(\log M) \propto M^{\Gamma}$. The slope, Γ , of the MF can be determined from

$$\Gamma = \frac{d \log N(\log m)}{d \log m} \quad (4)$$

where $N \log(m)$ is the number of stars per unit logarithmic mass. In the case of known values of age, reddening, distance and metallicity, the masses of probable members of any cluster can be determined by comparing their observed magnitudes with those predicted by a stellar evolutionary model. The MF determined for the cluster is given in Table 4. The effect of field star contamination is negligible for estimation of MF due to fact that most probable members (MPMs) are used for this purpose in the present study. Figure 6 shows the MF in the cluster fitted for the MS stars with masses $1.104 \leq M/M_{\odot} < 2.345$. The error bars have computed assuming Poisson statistics. The MF slope (Γ) for cluster comes out to be -1.06 ± 0.09 , which is low compared to Salpeter MF slope of -2.35 [23]. The obtained value of slope is close to the unity. An unit MF slope of a cluster corresponds to a uniform distribution of mass between small and large scales.

6.2. Mass segregation

The stellar encounters of the cluster's members cause mass segregation. In the processes of mass segregation, the higher-mass cluster members gradually sink towards the cluster centre by transferring their kinetic energy to the more numerous lower-mass stellar members of the cluster [24]. With the dynamical evolution of the cluster, the spatial mass distribution in the cluster changes with time. To investigate the dynamical evolution and mass segregation process in the cluster IC 361, the cumulative radial stellar distribution of the probable members for various mass ranges is shown in Fig. 7 and also given in Table 5. It is seen that MS slope does not become steeper as the radial distance from the cluster increases. This clearly suggests

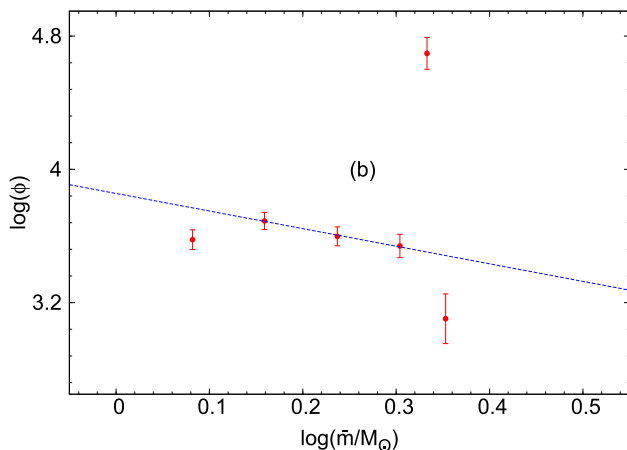


Fig. 6 The variation of logarithm MF with the logarithm of average mass of members

that the mass segregation is not taking place in the cluster. To further study the mass segregation in more detail, we plot the variation of mean mass along the radial distance for the probable members in Fig. 8. The average mass of centre bin is high, as expected.

Our study indicates that the higher and lower mass stars are uniformly distributed in the cluster region. To understand whether it is an imprint of star formation process in the clusters and/or result of dynamical evolution, we determined dynamical relaxation time, T_R , which is the time in which individual stars in the cluster exchange energies and their velocity distribution approaches Maxwellian equilibrium. It can be expressed as

$$T_R = \frac{8.9 \times 10^5 (NR_h^3/\bar{m})^{1/2}}{\log(0.4N)} \quad (5)$$

where T_R is in Myr, N is the total number of cluster members, R_h is the radius (in parsecs) containing half of the cluster mass and \bar{m} is mean mass of the cluster members in solar units [25]. We estimated a total of 1362 member stars in the mass range $0.93 \leq M/M_{\odot} < 2.4$. The total mass of the cluster is found to be $\sim 2198.95M_{\odot}$ for IC 361, which gives an average mass of $\sim 1.61M_{\odot}$ per star. The contribution of the low-mass stellar population is critical for constraining the total cluster mass, which is crucial in understanding the dynamical evolution and the long-term survival of a cluster [26]. It can be seen that the half-radius of the cluster, R_h , plays an important role in the determination of the dynamical relaxation time, T_R . To

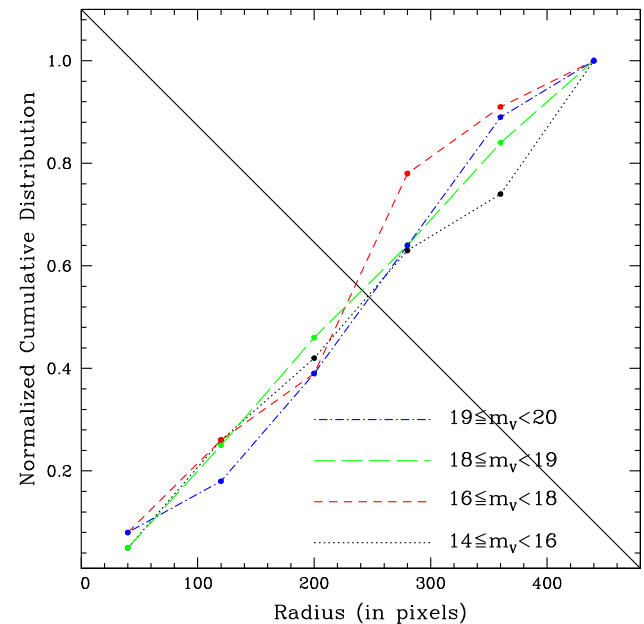
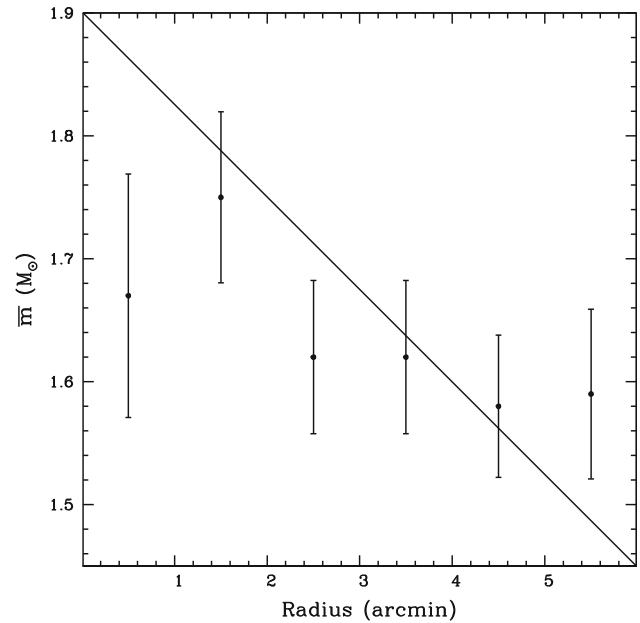


Fig. 7 The cumulative radial distribution of stars in various magnitude ranges of IC 361

Table 5 The estimated normalized cumulative distribution of probable members of IC 361 in various stellar magnitude groups

Zone size (in pixels)	Number of stars	Cum. stellar no.	Norm. cum. distribution
$14 \leq m_V < 16$			
000–080	001	001	0.05
080–160	004	005	0.26
160–240	003	008	0.42
240–320	004	012	0.63
320–400	002	014	0.72
400–480	005	019	1.00
$16 \leq m_V < 18$			
000–080	029	029	0.08
080–160	071	100	0.26
160–240	047	147	0.39
240–320	048	295	0.78
320–400	051	346	0.91
400–480	032	378	1.00
$18 \leq m_V < 19$			
000–080	012	012	0.05
080–160	042	054	0.25
160–240	047	101	0.46
240–320	040	141	0.64
320–400	042	183	0.84
400–480	036	219	1.00
$19 \leq m_V < 20$			
000–080	019	019	0.08
080–160	026	045	0.18
160–240	052	097	0.39
240–320	060	157	0.64
320–400	063	220	0.89
400–480	027	247	1.00

determine the R_h , author has estimated the radial distance of each member from the centre of cluster with mass. In this connection, members are arranged in the ascending order with respect to the radial distance and calculated the cumulative mass for the radial distance of each member. The cumulative mass of farthest member of cluster is equal to the total mass of cluster. The radial distance of a star, having cumulative mass equal to the half of total mass of cluster, is taken as the half mass radius of studied cluster. We obtained a half-mass radius for the cluster as 1.00 pc, which is $\sim 54.8\%$ of the cluster radius. A half-mass radius larger than half of the cluster radius suggests that the inner region still has a deficiency of massive stars in the core region of the cluster. We estimated the dynamical relaxation time $T_R = 9.46$ Myr for the cluster. T_R determined in the present study is much less than the present age of about

**Fig. 8** The mass distribution of stars in the radial direction

1.3 Gyr, which suggests that cluster IC 361 is dynamically relaxed.

7. Results and discussion

Open clusters are important tools for understanding of the evolution phenomenon in galaxies because they provide information on star formation history. In the present study, we have constructed a complete $UBVRIJHKW_1W_2$ catalogue for the cluster IC 361 by supplementing our photometric data with the 2MASS NIR and WISE mid- IR surveys. Using a V -band data of the present catalogue for the stars brighter than $V = 18$ mag, we found that the core and cluster radius are 2.0 ± 0.4 arcmin and 8.0 ± 0.5 arcmin, respectively. Using probable members, we derived the reddening in optical band using $(U - B)/(B - V)$ diagram and in NIR band using $(V - K)/(J - K)$ diagram. The values of reddening were obtained as $E(B - V) = 0.56 \pm 0.10$ mag and 0.62 ± 0.03 mag in optical and NIR , respectively. Since IC 361 shows a differential extinction across the cluster region as well as IR colour excess, it indicates that the stars are still embedded in the parent molecular gas and dust.

Based on the $(B - V)/V$ and $(V - I)/V$ CMDs and a visual fitting of isochrones for solar metallicity given by Marigo et al. (2008) to the blue sequence on the CMD, we determined a distance of 3.22 ± 0.07 kpc and $\log(\text{age})$ of 9.10 ± 0.05 for the cluster IC 361. At this distance, we estimated a respective core and cluster radii of 1.87 ± 0.18 pc and 7.50 ± 0.94 pc for this cluster. We estimated the

average total-to-selective extinction value as 2.94 ± 0.11 that is low compared to the normal value but in a reasonable agreement. The mean proper motion of the cluster was determined using the PPMXL catalogue and found to be 4.97 ± 0.17 mas/yr and -5.80 ± 0.18 mas/yr in the direction of RA and DEC, respectively. The MF slope of probable stars of the cluster is found to be 1.06 ± 0.09 in the mass range $1.10 \leq M/M_{\odot} < 2.34$.

8. Conclusion

The physical parameters of IC 361 are derived under this study. The membership analysis of IC 361 indicates least percentage of probable and statistical cleaned members at fainter limits of extracted stellar sequence within the field of view (FOV) of cluster. In the case of IC 361, we have not found any evidence of a steeper MF slope with the radial distance, which suggests that the mass segregation does not take place in the cluster. The relaxation time of the cluster has found to be much lower than its age, which implies that the cluster has long ago dynamically relaxed.

Acknowledgements GCJ is also acknowledged to ARIES, Nainital for providing observing facility duration from October 2012 to April 2015. GCJ is thankful to Honourable Dr. A.K. Pandey, Director, ARIES (Nainital) to permit him to use the gathered raw data of candidate through the letter No. AO/2018/41 on date April 12, 2018. This publication made use of data products from the Two Micron All Sky Survey, which is a joint project of the University of Massachusetts and the Infrared Processing and Analysis Center/California Institute of Technology, funded by the National Aeronautics and Space Administration and the National Science Foundation. This publication also makes use of data products from the Wide-field Infrared Survey Explorer, which is a joint project of the University of California, Los Angeles, and the Jet Propulsion Laboratory/California Institute of Technology, funded by the National Aeronautics and Space Administration.

References

[1] J Piccirillo and W L Stein *Astron. J.* **83** 971 (1978)

- [2] J Zdanavicius, R P Boyle, F J Vrba, K Zdanavicius and R Bartasiute *IAU Symp.* **266** 557 (2009)
- [3] J Zdanavicius, R Bartasiute, R P Boyle, F J Vrba and K Zdanavicius *Baltic Astron.* **19** 63 (2010)
- [4] A U Landolt *AU Astron. J.* **104** 340 (1992)
- [5] P B Stetson *Publ. Astron. Soc. Pac.* **99** 191 (1987)
- [6] I King *Astron. J.* **71** 64 (1966)
- [7] C Sneden, R D Gehrz, J A Hackwell, D G York and T P Snow *Astrophys. J.* **223** 168 (1978)
- [8] R Chini and W F Wargu *Astron. Astrophys.* **227** 213 (1990)
- [9] E L Wright, P R M Eisenhardt, A K Mainzer et al. *Astron. J.* **140** 1868 (2010)
- [10] Y C Joshi, L A Balona, S Joshi and B Kumar *Mon. Not. R. Astron. Soc. (MNRAS)* **437** 804 (2014)
- [11] Schmidt-Kalar Th., In: *Landolt/Bornestein, Numerical Data and functional Relationship in Science and Technology. Scaifers K, Voigt HH., (editors) Springer-Verlog, Berlin; New Series, Group VI.* **26** 14 (1982)
- [12] J F Dean, P R Warren and A W J ousins *Mon. Not. R. Astron. Soc.* **183** 569 (1978)
- [13] R L Phelps and K A Janes *Astrophys. J. Suppl. Ser.* **90** 31 (1994)
- [14] S Lata, A K Pandey, R Sagar and V Mohan *Astron. Astrophys.* **388** 158 (2002)
- [15] A R Walker *Mon. Not. R. Astron. Soc.* **213** 889 (1985)
- [16] G C Joshi and R K Tyagi *Mon. Not. R. Astron. Soc. (MNRAS)* **455** 785 (2016)
- [17] D C B Whittet and I G van Breda *Mon. Not. R. Astron. Soc.* **192** 467 (1980)
- [18] P Marigo, L Girdardi, A Bressan, M A T Groenewegen, L Silva and G L Granato *Astron. Astrophys.* **482** 883 (2008)
- [19] G C Joshi, Y C Joshi, S Joshi, S Chowdhury and R K Tyagi *Publ. Astron. Soc. Aust. (PASA)* **32** 22 (2015)
- [20] S Roeser, M Demleitner and E Schilbach *Astron. J.* **139** 24440 (2010)
- [21] R Sagar and T Richtles *Astron. Astrophys.* **250** 324 (1991)
- [22] S Sharma, A K Pandey, K Ogura, T Aoki, K Pandey, T S Sandhu and R Sager *Astron. J.* **135** 1934 (2008)
- [23] E E Salpeter *Astrophys. J.* **121** 161 (1955)
- [24] R D Mathieu and D W Latham *Astron. J.* **92** 1364 (1986)
- [25] L Jr Spitzer and M H Hart *Astrophys. J.* **164** 399 (1971)
- [26] R deGrijs and G Parmentier *Chin. J. Astron. Astrophys.* **7** 155 (2007)

Publisher's Note Springer Nature remains neutral with regard to jurisdictional claims in published maps and institutional affiliations.